applied sciences

MDPI

Article

Three-Dimensional Numerical Simulation of the Water Flow Effect on a Temporary Pier with Three Columns in Series

Zhongchu Tian and Zhangying Liao *

School of Civil Engineering, Changsha University of Science & Technology, Changsha 410076, China; tianzhongchu1@163.com

* Correspondence: zhyliao@hotmail.com

Abstract: In order to ensure the safety of temporary piers during bridge construction, it is necessary to analyze the water flow effects on temporary piers during flood periods. Based on the practical engineering of a new bridge in Jiangxi province, a three-dimensional numerical model was established using the Reynolds Time Average Navier–Stokes equation (RANS) and SST k-ω turbulence model to simulate the flow force on three-column temporary piers in series. The stress state of the temporary pier was obtained under different flow velocities and submergence depths. The distribution characteristics of the flow field around the temporary pier and the flow force characteristics acting on the temporary pier were analyzed and compared with the monitoring measurement data and the Morison equation calculation data. The results indicate that the local flow was accelerated on both sides of the temporary pier, but the local acceleration effect along the river flow direction was weakened. The flow velocity of the water around the temporary pier decreases with the increasing of river depth. The pressure on the outer surface of the temporary pier is basically negative pressure, except for the positive pressure on the upstream side. The absolute value of the negative pressure on both sides is much greater than the positive pressure on the upstream side. As the submergence depth and flow velocity increase, the pressure in each area gradually increases. The pressure distribution of the upstream pier is basically symmetrical, while the pressure distribution of the middle and downstream piers is asymmetric due to the influence of the vortex shedding from the front pier, resulting in a change in the water flow incidence point. The turbulence intensity in each region of the flow field shows a trend of first increasing and then decreasing with the depth of the water flow. The drag coefficient and lateral force coefficient of the temporary pier are basically not affected by the inflow velocity, but the resistance and lateral force increase with the increase in submergence depth and inflow velocity.

Keywords: highway bridges; temporary pier; field measurement; numerical simulation; water flow force; water flow velocity; surface pressure; turbulence intensity

check for updates

Citation: Tian, Z.; Liao, Z. Three-Dimensional Numerical Simulation of the Water Flow Effect on a Temporary Pier with Three Columns in Series. *Appl. Sci.* **2023**, *13*, 11683. https://doi.org/10.3390/app132111683

Academic Editors: Satoru Okamoto and Junhong Park

Received: 4 August 2023
Revised: 5 October 2023
Accepted: 23 October 2023
Published: 25 October 2023

Copyright: © 2023 by the authors. Licensee MDPI, Basel, Switzerland. This article is an open access article distributed under the terms and conditions of the Creative Commons Attribution (CC BY) license (https://creativecommons.org/licenses/by/4.0/).

1. Introduction

With the rapid development of bridge construction technology, in order to ensure that the construction period does not affect existing traffic, incremental launching construction technology has been widely adopted. During the incremental launching construction of long-span bridges, the spacing between main piers is large. In order to ensure construction safety, temporary piers need to be set between the main piers. When water flows through the pier columns, flow separation, vortex shedding and other phenomena will occur, which will lead to an increase in the force on the temporary piers. When the water flow speed is high, the resulting water flow force may become an important component of force on the temporary piers. The fatigue failure of the temporary piers caused by the bypass flow may also lead to instability and collapse of the bridge.

In previous studies, scholars conducted relevant research on the hydraulic characteristics of engineering structures such as cofferdam structures [1,2], bridge substructures [3]

and toothed-component mixed embankment overturning [4]. The difference in the three-dimensional wake between square and circular sections was examined by Agbaglah et al. [5]. In the study of flow around cylinders [6–9], through the numerical simulation of tandem double cylinders, it is found that the spacing ratio has a significant effect on the shedding flow pattern, the lift drag coefficient and the Strouhal number. Deng et al. [10] carried out a cylindrical flow tank experiment, and obtained the effect of the spacing ratio on the near wall tandem double cylinders. Zhou et al. [11] verified the existence of critical spacing. Zou et al. [12] studied the flow characteristics of tandem double corrugated cylinders. For the study of parallel double cylinders, the influence of the spacing ratio on wake vortices, cylinder hydrodynamic coefficients, double cylinder interaction effects and flow field characteristics was analyzed via numerical and experimental research [13–17]. Ma et al. [18] obtained the energy distribution of the wake field around two parallel cylinders. Harichandan and Roy [19] pointed out the frequency of the cylinder and the flow field. Tan et al. [20] and Tu et al. [21] analyzed the characteristics of three series columns. Yang et al. [22] studied the critical spacing of three cylinders in series. Zhang et al. [23] studied the vortex-induced vibration of three consecutive cylinders with different spacing ratios.

In the design of temporary pier structure, according to the "*General Code for Design of Highway Bridges and Culverts*" [24], the flow force of a single pile column can be simply calculated. However, there is no stipulated calculation method for the flow effect of series three-column temporary pier structures, and the code does not consider the lateral force caused by vortex shedding and the lifting effect on the structure under the action of water flow. The API [25] specification in the United States uses the Morison equation to calculate water flow force. The Morison equation itself is a semi-empirical formula, which is not convenient for direct application. The value of the parameters in the Morison equation directly determines the accuracy of the calculation, and there are some limitations in the current method of parameter selection.

In summary, the current research on the flow around these cylinders has reference value for us to calculate the water flow force on temporary piers. However, in practical engineering, the value of water flow force is related to various parameters of the bridge (cross section type, column spacing, etc.), so the water flow force acting on a specific structure is worth studying. However, there is currently very little research on the water flow effect on temporary piers; the existing design specifications do not fully consider the water flow force effect of temporary piers. During the construction stage, it is necessary to accurately calculate the water force acting on the temporary pier to guarantee construction safety. On the other hand, previous studies have mostly focused on the dynamic response of the structure under water flow, and have not studied the hydrodynamic characteristics of the three-dimensional flow field around the structure and the mechanism of local scour in detail. At present, there are few studies on the flow around a cylinder under conditions of high Reynolds numbers. In practical engineering, the cylinder is large-scale and has a high Reynolds number; therefore, in order to ensure the construction safety of large bridges and the navigation safety of ships when the flow rate is high in the flood period, it is necessary to conduct numerical simulation and analysis of the characteristics of the surrounding flow field as well its effect on the mechanical behaviors of temporary piers in practical projects.

In previous studies, a large number of scholars have used the LES and RANS methods to conduct numerical simulations on the fluid [26]. Francesco et al. [27] used the LES method to deal with high Reynolds and Mach number flow with adverse pressure gradient conditions. Yang et al. [28] studied the applications in transient flows and gas turbine combiner flows of the LES method. Chipongo et al. [29] studied the robustness and accuracy of the RANS model in complex turbulence in open channels subjected to lateral inflow and proved that the RANS model agrees well with the experimental water surface profile, which is superior to current theoretical methods used for design purposes. Hanjalic et al. [30] also confirmed the important role of RANS, especially in industrial and environmental computing. Lamberti et al. [31] believe that RANS solvers, especially those based on standard eddy current viscosity models (such as K-ε, K-ω, S-A and K-ω SST), are expected

to be the main approach of flow CFDs with high Reynolds number for decades. Because LES requires higher simulation complexity and greater computational costs, it may even produce less accurate and less reliable results than RANS. In the present study, firstly, the numerical model of the temporary pier subjected to flow force during the bridge jacking construction was established considering the effects of Renault time mean and SST k-ω turbulence. then the flow field and flow force characteristics around the temporary pier were analyzed and finally the simulated results were compared and validated with those obtained via existing specifications.

2. Project Overview

The researched bridge crosses the Ganjiang River, which is located in the north of Ganzhou. The superstructure of the main bridge is a four span continuous steel truss with a total length of 1543 m. According to the navigation investigation (Class II waterway), the water flow speed during the flood period is 4 m/s, and the elevation of the flood level for a 20-year return period is 102.45 m. The lowest and normal elevation of the riverbed at the location of the temporary pier is 83.6 m and 94.11 m, respectively. Due to the constraints of navigation requirements and on-site construction conditions, an incremental launching construction method for the main girder of the bridge is adopted. During the launching construction stage, temporary piers need to be set up between the bridge piers; thus, construction platforms and launching equipment can be arranged above the temporary piers.

The temporary pier is composed of steel pipe pile foundations and the corresponding longitudinal and transverse distribution beams. The structural form is shown in Figure 1. Three rows of steel columns are arranged along the transverse direction of the bridge. The steel columns of the temporary pier are made of steel pipes with a diameter of 1200 mm and a wall thickness of 16 mm.

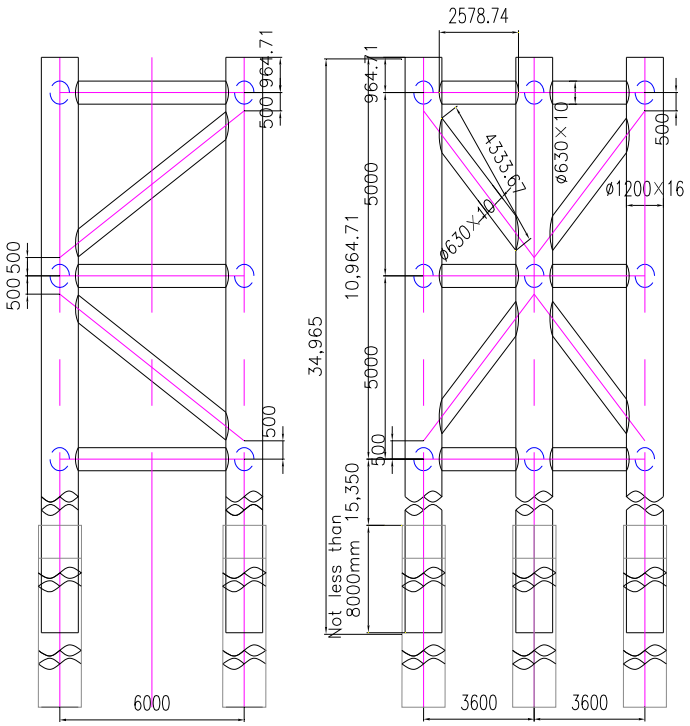


Figure 1. Schematic diagram of the elevation and cross-section of the temporary pier (unit: mm, ϕ represents the diameter).

3. Numerical Simulation

3.1. Theoretical Model

The Navier–Stokes equation of incompressible viscous fluid under the Arbitrary Lagrange–Euler (ALE) description is used and expressed as follows:

$$\frac{\partial u_j}{\partial x_j} = 0 \tag{1}$$

$$\frac{\partial \rho u_i}{\partial t} + \frac{\partial \rho u_i u_j}{\partial x_j} = -\frac{\partial \rho}{\partial x_i} + \frac{\partial}{\partial x_{ij}}\left[\mu + \mu_r\left(\frac{\partial u_i}{\partial x_j} + \frac{\partial u_j}{\partial x_i}\right)\right] \tag{2}$$

where u_i and u_j are velocity components and ρ is fluid density.

To solve these equations, a turbulence model was introduced. Because the SST k-ω model proposed by Menter is a combined turbulence model with k-ε and k-ω, the SST k-ω turbulence model adopts the k-ω turbulence model in the near-wall area, and the k-ε turbulence model in the expected free shear layer in the external wake region. Nguyen et al. [32] compared the k-ε, k-ω and k-ω SST methods and found that the SST k-ω model was more suitable for studying the turbulent flow state around the cylinder. Therefore, the SST k-ω model is used to simulate the cylindrical winding flow condition, which is presented as follows:

$$\frac{\partial \rho k}{\partial t} + \frac{\partial \rho u_j k}{\partial x_i} = \frac{\partial}{\partial x_j}\left[(\mu + \sigma_k \mu_r)\frac{\partial k}{\partial x_j}\right] + \tau_{ij}\frac{\partial u_i}{\partial x_i} - \beta^* \rho k \omega \tag{3}$$

$$\frac{\partial \rho \omega}{\partial t} + \frac{\partial \rho u_i \omega}{\partial x_j} = \frac{\partial}{\partial x_j}\left[(\mu + \sigma_m \mu_r)\frac{\partial \omega}{\partial x_j}\right] + \frac{\gamma}{\nu_r}\tau_{ij}\frac{\partial u_i}{\partial x_i} - \beta\omega^2 + 2\rho(1 - F_1)\frac{\sigma_{\omega 2}\partial k \partial \omega}{\omega \partial x_i \partial x_j} \tag{4}$$

where F_1 is the mixed function; depending on the meshing of the model, it can be calculated as follows:

$$F_1 = \tanh(\gamma_1^4) \tag{5}$$

$$\gamma_1 = Min[Max(\frac{\sqrt{k}}{\beta^* \omega y}, \frac{500\nu}{y^2 \omega}), \frac{4\rho\sigma_{\omega 2} k}{CD_{k\omega} y^2}] \tag{6}$$

$$CD_{k\omega} = Max(2\rho\sigma_{\omega 2}\frac{1}{\omega}\frac{\partial k}{\partial x_j}\frac{\partial \omega}{\partial x_j}, 10^{-10}) \tag{7}$$

where $\sigma_{\omega 1} = 2.00$, $\sigma_{\omega 2} = 1.186$ and $\beta^* = 0.09$.

3.2. Numerical Model

The calculation domain of the numerical model is shown in Figure 2. The speed is used as the inlet boundary condition of the model, and the pressure is used as the outlet boundary condition of the model. The non-slip wall surface is used as the boundary condition between the surface of the temporary pier and the bottom wall and the top, the left and the right surfaces are set as symmetric boundary conditions. The spacing between the centers of adjacent temporary piers is 3D; D is taken as 1.2 m; the distance between the center of the temporary pier and the symmetrical boundary is 10D; the distance between the center of the upstream/downstream temporary pier and the entrance/exit boundary is 10D/25D, respectively. The flow rate considers a total of five flow rates: 2, 2.5, 3, 3.5, 4 m/s; three typical depths of 10, 15 and 20 m were selected for the submerged depth; in total, there were 15 working conditions.

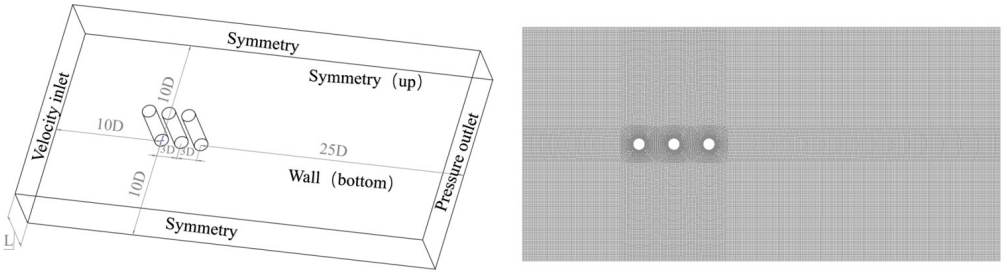


Figure 2. Calculation domain and grid division.

The calculation model takes the center of the upstream pier as the coordinate origin, the downstream direction is the x-axis direction, the y-axis direction is perpendicular to the flow direction and the flow depth direction is the z-axis direction. A hexahedral-structured grid with a size of 0.2 mm was used to mesh the model. The grid around the cylinder and the wake area are refined to improve the accuracy of the numerical calculation. For example, the grid of 0.5 times the spacing between columns around the cylinder is refined, the gradient rate of the grid in the refined area is 1.07 and the first layer of the grid perpendicular to the wall is $y^+ = 1$.

3.3. Parameter Selection and Model Correctness Verification

The Reynolds number represents the relationship between inertial force and viscous force, and is the main factor determining the state of the fluid flow. Inertial force plays a primary role at a high Reynolds number; viscous force plays a major role at a low Reynolds number. The expression is:

$$\mathrm{Re} = \frac{\rho u D}{\mu} = \frac{u D}{\nu} \tag{8}$$

ρ is fluid density, u is fluid velocity, D is the diameter of the circular cylinder and ν and μ are the kinematic viscosity and the dynamic viscosity of the fluid, respectively, $u = \mu/\rho$. The fluid is set to water with a density ρ = 1000 kg/m^3, and a dynamic viscosity coefficient μ = 0.001003 kg/(m·s).

The Strouhal number St represents the relationship between the cylindrical diameter, the frequency of vortex shedding and the fluid velocity. The expression is

$$St = \frac{fD}{u} \tag{9}$$

where

f is the frequency of vortex shedding and D is the diameter of the cylinder.
C_l and C_d are the lift coefficient and the drag coefficient, respectively, whose value depends on the characteristics of the cylinder surface and the Reynolds number. The expression is

$$C_l = \frac{2F_l}{\rho U^2 S} \tag{10}$$

$$C_d = \frac{2F_d}{\rho U^2 S} \tag{11}$$

where U is the fluid velocity; ρ is the fluid density; S is the downstream projection area of the submerged part of the temporary pier; F_l and F_d are resistance perpendicular to the flow direction and resistance in the downstream direction, respectively, namely the lift and resistance of the cylinder.

Table 1 analyzes the influence of the grid size, the influence of the time step on the resistance coefficient and the influence of the Strouhal number when flowing around a single cylinder. The results $\overline{C_d}$ and S_t with a grid size of 0.5 mm are slightly larger than those with grid sizes of 0.2 mm and 0.1 mm. Furthermore, the results of 0.2 mm and

0.1 mm are close to each other and close to the results of Ouvard et al., and Meyers et al. Considering the precision and efficiency, a grid size of 0.2 mm and a time step of 0.001 s were chosen for subsequent numerical simulations. By comparing with the existing data in the literature, we find that the average resistance coefficient of the calculated value and number are close to the calculated values of Ouvard [33] and Meyers [34].

Table 1. Grid independence and model correctness verification.

Case	Reynolds Number/10^3	Grid Size/mm	Dimensional Time Step $\Delta t/s$	$\overline{C_d}$	S_t
C1	20	0.5	0.01	1.08	0.231
C1	20		0.001	1.07	0.229
C2	20	0.2	0.01	1.06	0.216
C2	20		0.001	1.05	0.215
C3	20	0.1	0.01	1.04	0.215
C3	20		0.001	1.05	0.213
Ouvard et al. [33]				1.03	0.219
Meyers et al. [34]				1.05	0.210

According to Hu's [35] research, the root mean square (RMS) of the lift coefficient is sensitive to numerical methods, turbulence models and grids, and can be used to capture the periodic characteristics and force action of vortex shedding. As shown in Figure 3, in order to further verify the model correctness, the flow rate range is expanded and compared with the existing literature [36,37] results to discuss the variation of the order cylinder winding flow at different Reynolds numbers. Due to the direct integral relationship between the lift coefficient and the pressure coefficient, the two dimensionless quantities can be directly verified to obtain a consistent change trend, which shows that the model can simulate the lift situation well with the Reynolds number. As shown in Figure 4, this paper compared the S_t numbers obtained using the method presented in this article with those obtained through experiments conducted by Norberg et al., and studied the vortex shedding phenomenon of a cylinder in water. It was found that the two sets of data were in good agreement, further verifying the reliability of the method used in this paper.

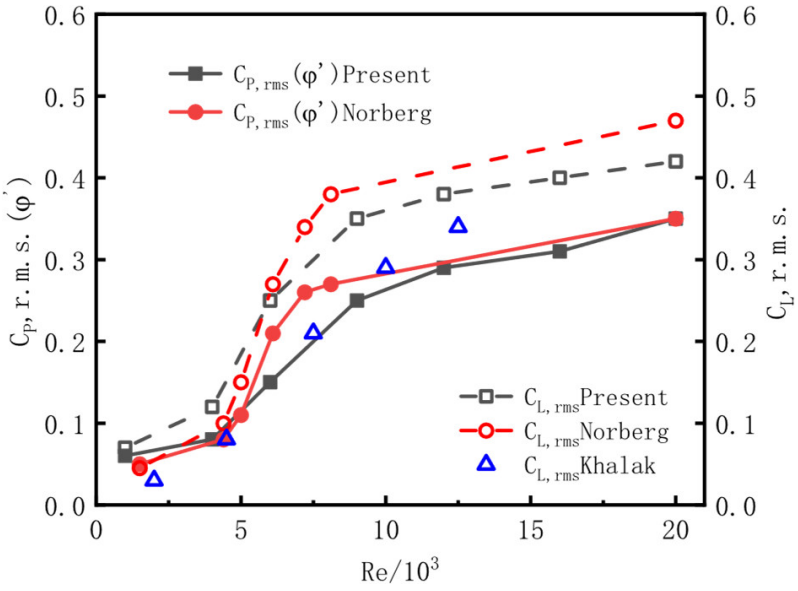


Figure 3. Verification of lift coefficient (φ′ is angle for maximum C_P, r.m.s).

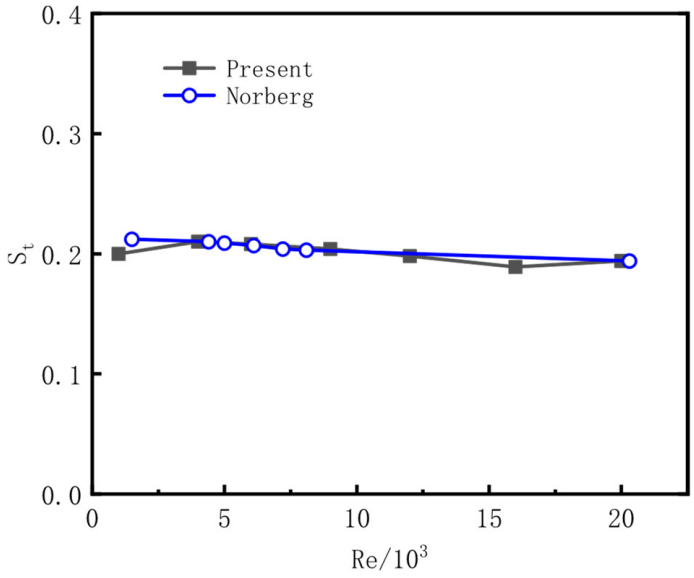


Figure 4. Verification of the Strouhal number.

4. Comparison between Numerical Simulation and Analytical Methods

Based on the established numerical model, the current theories for calculating water pressure can refer to the "Load Code for Harbour Engineering" [38], "Technical Specifications for Construction of Highway Bridges and Culverts" [39] and the Morison equation. Luo et al. [40] have proven that the water pressure calculated via the Morison equation is on the safe side and reliable in high-flow-velocity regions. Therefore, this article uses the Morison equation to calculate the water pressure of three column piers.

4.1. The Morison Equation Is Used by Calculating the Water Pressure

The Morison equation is one of the most commonly used methods for analyzing the forces on small-diameter rigid columns under the action of water flow. It assumes that the structure has no elastic deformation under the action of water flow, so the water flow force on rigid structures is only related to the incoming water flow. The Morison equation was applied to theoretically calculate the water pressure acting on temporary piers. The Morison equation assumes that the water pressure at any height of the structure consists of two parts: drag force f_D and inertia force f_t:

$$F = f_D + f_t = \frac{1}{2} C_D \rho A (u_x - u_t)|u_x - u_t| + C_M \rho V_0 \left(\frac{du_x}{dt} - \frac{du_t}{dt}\right) \quad (12)$$

where u_x is the water flow velocity, $\frac{du_x}{dt}$ is the water flow acceleration, u_t is the structural velocity and $\frac{du_t}{dt}$ is the structural acceleration.

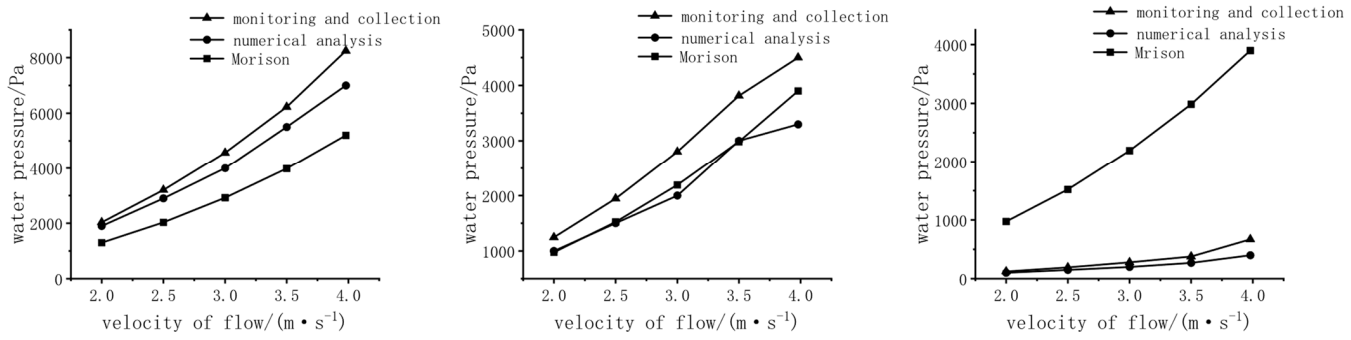
In this study, the water flow is assumed to be uniform, and the vibration velocity of the temporary pier under the impact of water flow is negligible in comparison with the water flow velocity. Therefore, the first item is mainly considered, where the water flow force is $\frac{1}{2} C_D \rho A(u_x)|u_x|$. C_D is the drag force coefficient, C_M is the inertia force coefficient and the values of C_D and C_M are clearly specified and explained in national regulations.

According to the Morison equation, the formula for calculating the flow pressure is $f = \frac{1}{2} C_D \rho(u_x)|u_x|$, where C_D is taken as 0.65 according to the American API specification, and the shielding factor is taken as 0.75.

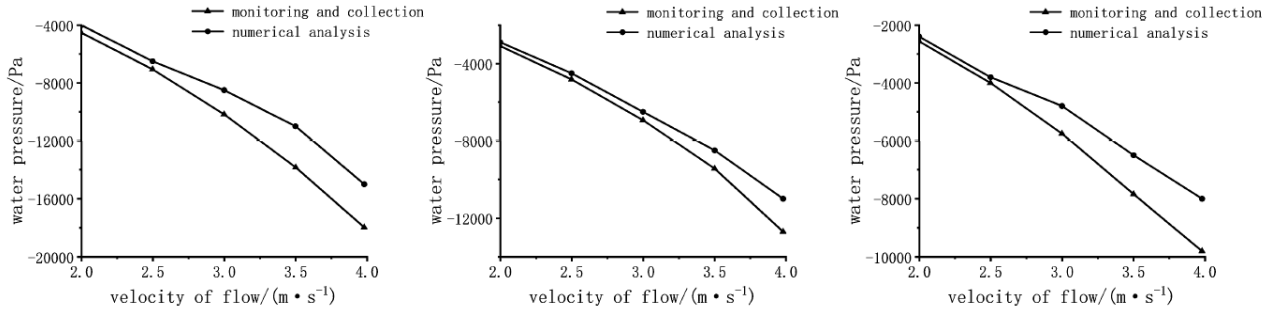
4.2. Data Comparison

As shown in Figure 5, A1, B1 and C1 represent the upstream, middle and downstream piers, respectively. The data obtained from the filed measurement, the numerical simulation and the calculation are compared. Except for the flow force along the incoming direction,

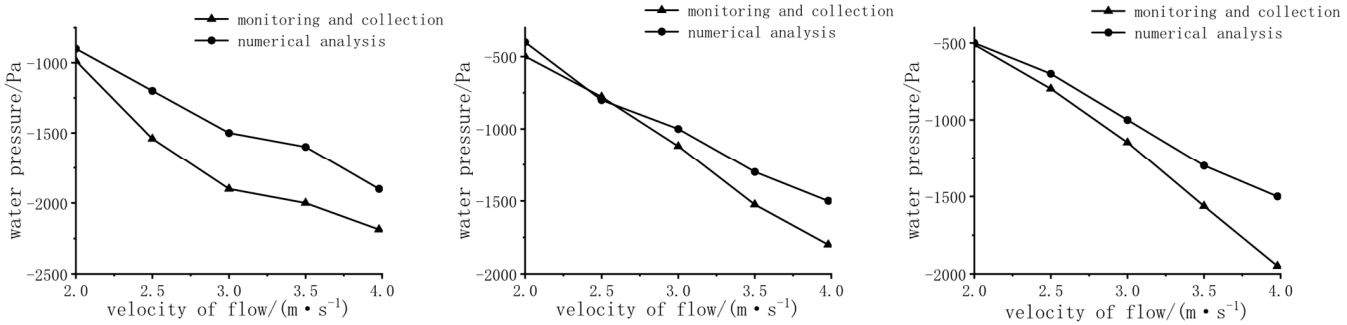
the lateral and back force of the temporary pier are negative due to the action of the lateral flow and the rear vortex, and the pressure increases on increasing the flow velocity. Compared with the resistant and lateral force, the absolute negative pressure on the side of these three piers is greater than the positive pressure against the incoming surface; thus, more attention should be paid to the structural design process. There is little difference between the measurement and numerical results, and the change pattern is basically similar.



(**a**) A1, B1 and C1 resistance



(**b**) A2, B2 and C2 lateral force



(**c**) A3, B3 and C3 backside force

Figure 5. Comparison of water pressure.

The average errors of water pressure on the temporary pier among the measurement results and those obtained via numerical simulation and the Morison equation for A1 are 10.2% and 36.3%, respectively, as shown in Table 2. The average errors for B1 are 7.9% and 20.0%, respectively. Due to the lack of detailed regulations on the shielding coefficient of three column piers in the specifications, the comparison with the Morison equation for the C1 pier is not provided. The numerical simulation results agree well with the measured ones for A1 and B1, indicating that the numerical method can accurately predict the water pressure.

Table 2. Average error of current research method and measured data of temporary pier.

Mean Error (%)	A1	B1	C1
Numerical simulation	10.2%	7.9%	10.5%
Morison equation	36.3%	20.0%	-

5. Numerical Results and Discussions

5.1. Water Force of Temporary Pier

The force of the temporary pier under the action of water flow can be divided into resistant and lateral force, respectively. The resistance is the force of the piers in the forward flow, and the lateral force is the force perpendicular to the flow acting on the temporary piers, which is expressed as F_d and F_l. C_l and C_d are the lift coefficient and the drag coefficient, respectively, whose values depend on the characteristics of the column surface and the Reynolds number.

Figure 6 shows the calculated lateral force and resistance, as well its coefficient of the upstream pier. The variation of the incoming flow speed and the depth of the temporary pier basically do not affect the lateral- and resistant-force coefficient. Under the same depth conditions, the lateral force and resistance increase with increasing flow velocity, and the greater the submerged depth, the more obvious this phenomenon is. At the same flow rate, the lateral force and resistance gradually increase with the submerged depth of the temporary pier.

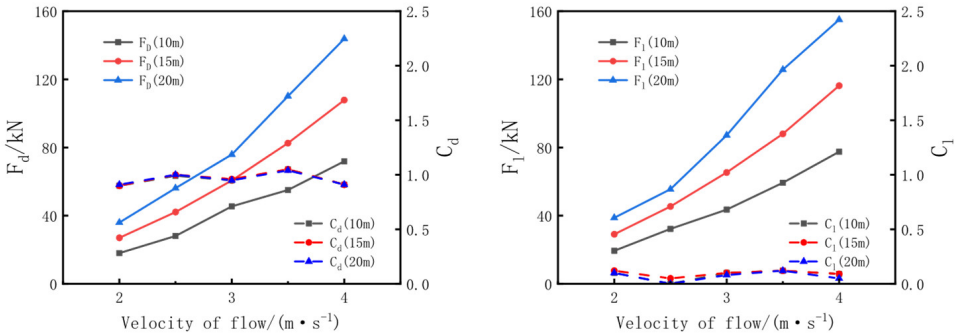


Figure 6. Flow force of the temporary pier.

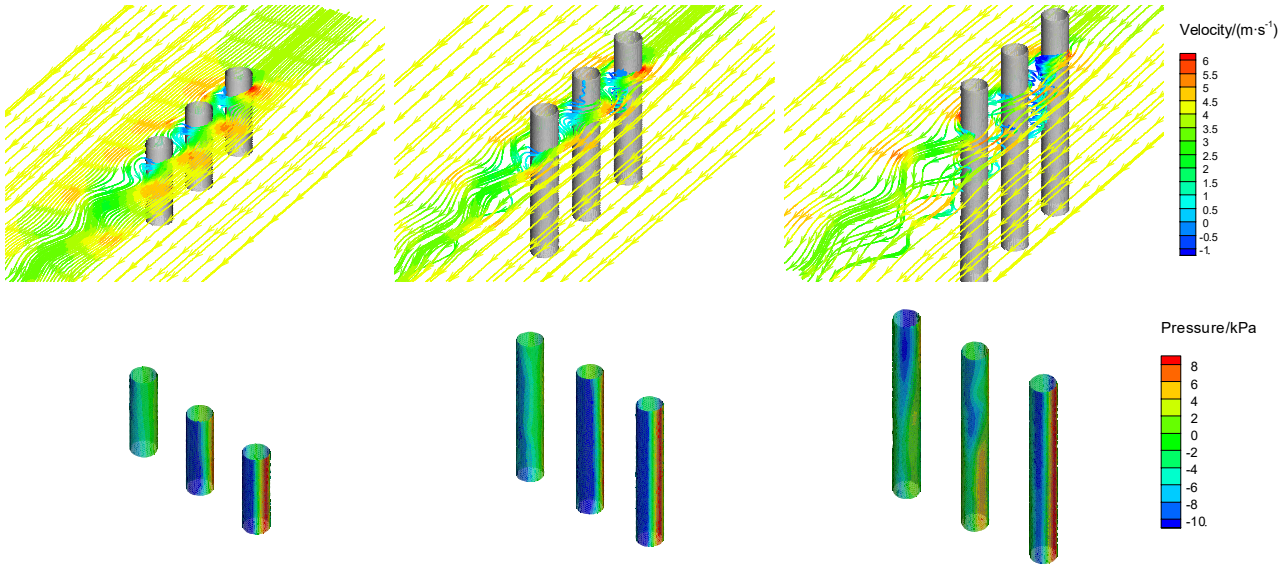
5.2. Surface Pressure of the Temporary Pier

When the river flow's speed is 4 m/s, the surface pressure distribution and flow field trace of temporary piers under different depths are shown in Figure 7. With the increase in the submerged depth of the temporary pier, the maximum positive pressure area on the outer surface of the upstream temporary pier gradually moves down, and the surrounding pressure is basically symmetrically distributed. According to the flow field characteristics, it can be seen that although there is a vortex after the upstream pier, this area has little influence on the pressure of the upstream pier, so the pressure around the upstream pier column is still symmetrically distributed along the central axis. Due to the small spacing among the three temporary piers, the flow will form a vortex behind the former pier, and the average flow rate in the vortex area is much less than the upstream flow rate of the temporary pier.

5.3. Speed and Pressure Field

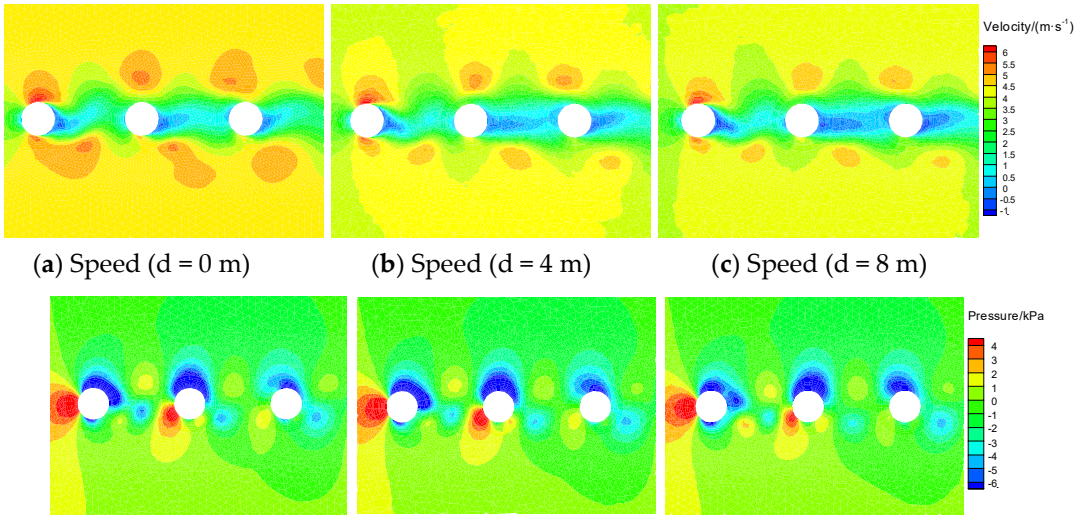
Figures 8 and 9 compare the speed field and pressure field of the temporary pier under the submerged depths of 10 m and 20 m, respectively. There is a local acceleration area near the temporary pier, and the maximum speed appears on both sides of the temporary pier. The deeper the water, the weaker the local acceleration effect. The flows generated by the three piers basically do not affect each other, and the velocity field around the three-column pier is basically consistent with that of a single column. When the water depth is 8 m,

the flow is affected by the bottom wall of the river and the pile column; thus, the flow changes from a two-dimensional distribution in front of the temporary pier to a three-dimensional distribution behind the pile column. With the decrease in the water depth, this three-dimensional disturbance is gradually weakened. The pressure field around the temporary pier remains basically unchanged in different water depths; the maximum positive pressure area appears on the side of the upstream pier. The range of the positive pressure area decreases, but the range of the negative pressure area is increased. Except for the upstream pier, the pressure field of other pier columns is disturbed to different degrees, but the form of the negative pressure in front of the pier and on both sides of the pier is basically unchanged.



(**a**) Submergence depth 10 m (**b**) Submergence depth 15 m (**c**) Submergence depth 20 m

Figure 7. Surface pressure and trace distribution around temporary pier.



(**a**) Speed (d = 0 m) (**b**) Speed (d = 4 m) (**c**) Speed (d = 8 m)

(**d**) Pressure (d = 0 m) (**e**) Pressure (d = 4 m) (**f**) Pressure (d = 0 m)

Figure 8. Speed field and pressure field (submerged depth of 10 m).

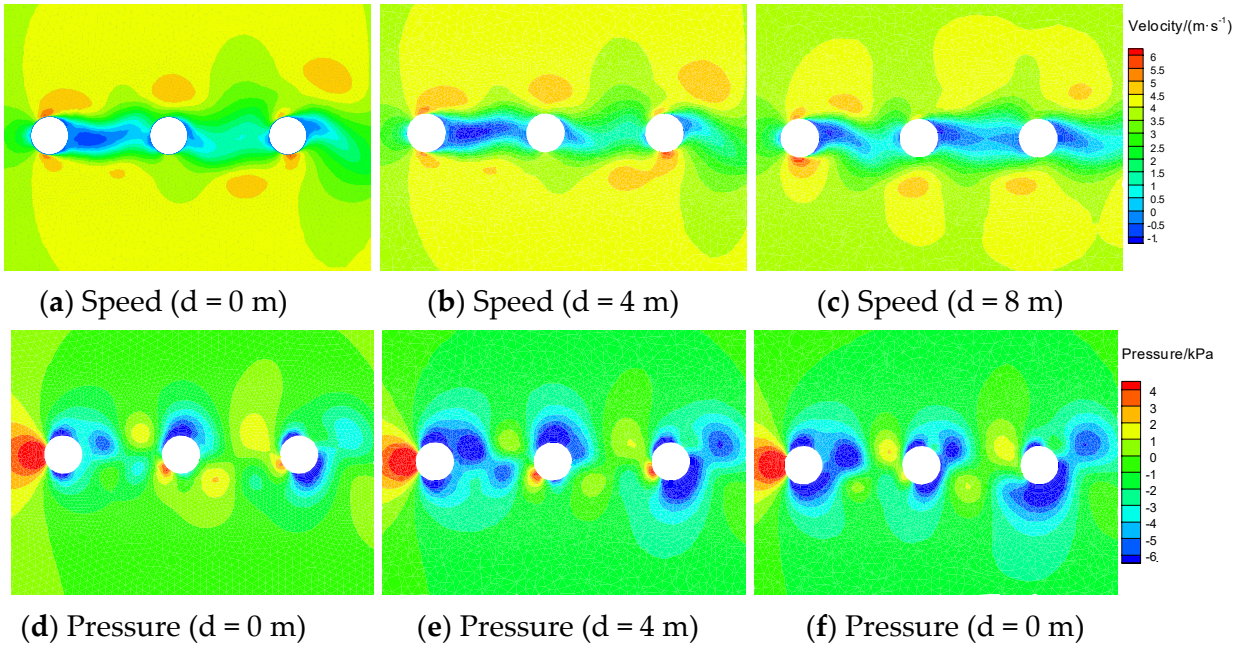


Figure 9. Speed field and pressure field (submerged depth of 20 m).

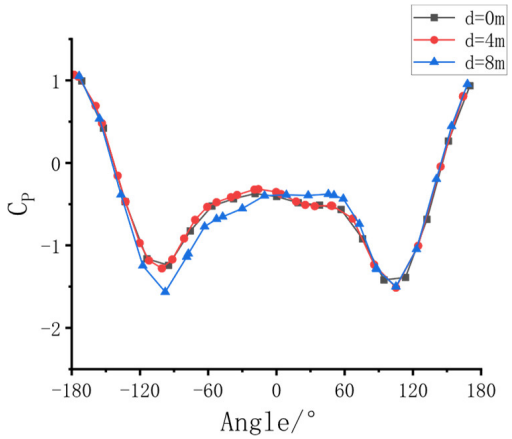
5.4. Surface Pressure Distribution

Figure 10 shows the distribution of the circumferential pressure coefficient on the surface at different sections along the water depth when the temporary pier is submerged at a depth of 20 m. The pressure around the upstream pier is symmetrically distributed with respect to x = 0°. According to the flow field characteristics of the upstream pier, although there is a vortex behind the upstream pier, this area has little influence on the pressure of the upstream pier. Therefore, the pressure around the upstream pier column is still distributed symmetrically along the central axis, and the pressure in the negative pressure area on both sides of the upstream pier and behind the pier does not change much. For the midstream pier, due to the influence of the vortex shedding behind the upstream pier column, the incident point of the water flow on the midstream pier changes, resulting in the maximum positive pressure appearing around −140° (left front) of the pier column. For the downstream pier, the position of the maximum positive pressure is near −150° (left front), where the pressure is not much different to the maximum pressure at the middle pier. In addition, the pressure of the downstream pier is less than that of the midstream pier, so that the resistance of the downstream pier is greater than that of the midstream pier. From Figure 10b,c, it can be seen that the pressure fluctuations around the middle and downstream piers are more obvious than those around the upstream piers, mainly due to the regular vortex shedding generated by the front pier columns. The circumferential pressure coefficient of the midstream pier in the section at d = 8 m fluctuated significantly, which is due to the influence of the bottom boundary on the fluid, resulting in uneven distribution of flow velocity along the water depth, leading to different shedding situations of the vortex at different depths. Therefore, the circumferential pressure coefficient distribution of the midstream pier varies significantly along the water depth.

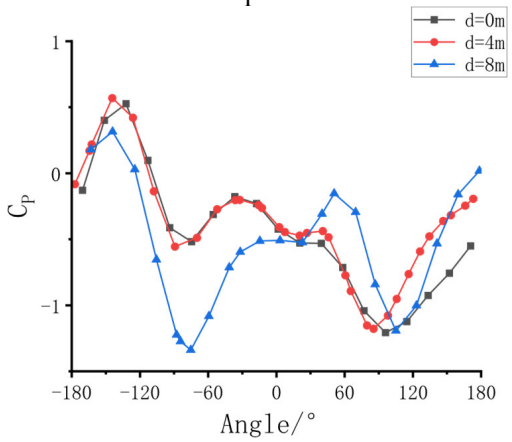
5.5. Turbulence Intensity

In Figure 11, taking a flow speed of 4 m/s as an example, the turbulent intensity distribution of the plane section at a depth of 2 m and the vertical section along the central axis of the temporary pier was depicted. When the submergence depth is 10 m, the turbulence intensity near the temporary pier is higher than that away from the temporary pier, and the maximum turbulence intensity occurs in the wake area of the downstream pier. As the depth of the flow increases, the overall turbulence intensity is first increasing

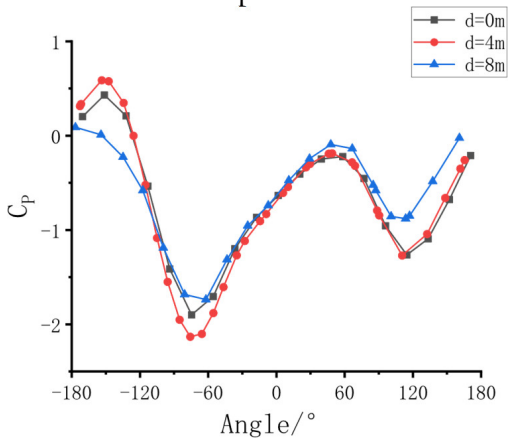
and then decreasing. When the temporary pier is submerged at a depth of 20 m, the overall turbulence intensity gradually decreases along the flow direction. The maximum turbulence intensity between the upper and middle stream pier is significantly enhanced in comparison with the temporary pier at the submerged depth of 10 m. This may be due to slow flow at the bottom of the temporary pier, which enhances the energy input of the main flow to the vortex shedding at the wake of the upstream pier.



(**a**) Distribution of circumferential pressure coefficient in upstream pier

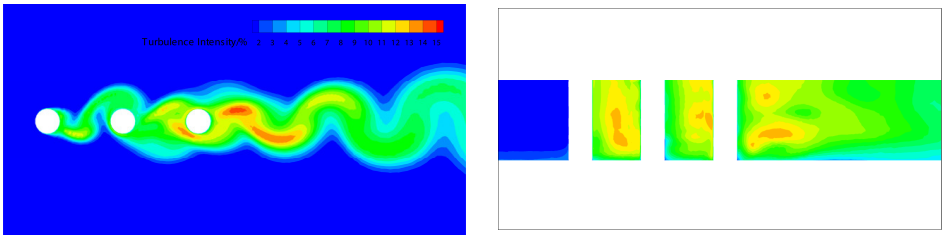


(**b**) Distribution of circumferential pressure coefficient in midstream pier

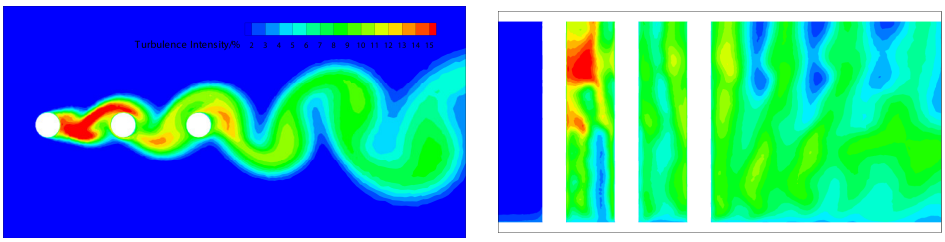


(**c**) Distribution of circumferential pressure coefficient in downstream pier

Figure 10. Distribution of circumferential axial pressure coefficient of temporary pier.



(**a**) Inundation depth of 10 m



(**b**) Inundation depth of 20 m

Figure 11. Turbulence intensity distribution.

6. Conclusions

This article takes the temporary pier of a truss bridge in Jiangxi as the research object; a three-dimensional model was established using the software Fluent (version 2022 R1) to investigate the interaction between water flow and the temporary pier, and the following conclusions were obtained:

1. The water flow characteristics of the temporary pier during the flood period were obtained through numerical simulation. When the water flows through the temporary pier, the vortex was generated behind it. This affects the distribution of water flow force around these three piers.
2. The water pressure obtained from a numerical analysis was smaller than that from measurement, but the overall difference is not significant. By comparing the numerical simulation, the filed measurement and the results of the Morison equation, we found that the numerical simulation results are closer to the measured value and the numerical simulation method is more reliable than the semi-empirical method; thus, numerical simulation can be used as an important tool for studying water flow forces.
3. The side of the temporary pier is subjected to significant negative pressure, which should be taken seriously in the structural design process.
4. The circumferential pressure of the upstream pier is approximately symmetrically distributed around 0°, while vortex shedding occurs at the midstream pier. The maximum positive pressure position of the midstream and downstream pier appears near -140° (left front) and -150° (left front), respectively.
5. The area with the highest turbulence intensity occurs between the upstream and midstream piers, and the turbulence intensity is affected by the flood depth.
6. Except for the positive pressure on the upstream side, the surface of the temporary pier is subjected to negative pressure, and the lift and drag coefficient are not affected by the flow velocity and submergence depth of the temporary pier.

Author Contributions: Conceptualization, Z.T.; methodology, Z.T.; software, Z.L.; validation, Z.T.; formal analysis, Z.L.; investigation, Z.L.; resources, Z.T.; data curation, Z.L.; writing—original draft preparation, Z.L.; writing—review and editing, Z.T. and Z.L.; supervision, Z.T.; project administration, Z.T. All authors have read and agreed to the published version of the manuscript.

Funding: This study is supported by the Key R&D Project of Ningxia Hui Autonomous Region (2021BEG02021).

Institutional Review Board Statement: Not applicable.

Informed Consent Statement: Not applicable.

Data Availability Statement: The data are not publicly available due to privacy.

Conflicts of Interest: The authors declare no conflict of interest.

References

1. Liu, Y.; Zhu, B.; Zhang, C.; Zhang, J. Experimental study on current force of dumbbell type occluded pile cofferdam. *Railw. Stand. Des.* **2020**, *64*, 72–76.
2. Zhang, C.; Zhu, B.; Zhang, Z.; Zhao, Y.; Song, F. Study on calculation method of a new type dumbbell composite cofferdam structure in deep water foundation. *J. Railw. Sci. Eng.* **2020**, *17*, 1957–1969.
3. Liu, T. Analysis of Force of Flow Around Single Column of Sea-Crossing Bridge. Ph.D. Thesis, Southwest Jiaotong University, Chengdu, China, 2018.
4. Bei, J.; Mou, Y. Numerical analysis of impacting factors for current force over gear-type mixture embankment. *Port Waterw. Eng.* **2022**, *593*, 94–99.
5. Agbaglah, G.; Mavriplis, C. Three-dimensional wakes behind cylinders of square and circular cross-section: Early and long-time dynamics. *J. Fluid Mech.* **2019**, *870*, 419–432. [CrossRef]
6. Chen, J.; Yu, P.; Ouyang, H. Frequency characteristics of the three-dimensional flow past tandem cylinders with unequal diameters. *Chin. J. Appl. Mech.* **2022**, *39*, 386–393.
7. Zhao, H.; Wang, C.; Ren, B.; Chen, W.; Wang, G. Numerical simulation of flow around two tandem cylinders at low Reynolds number using FDM-VBF. *J. Dalian Univ. Technol.* **2022**, *62*, 292–298.
8. Du, X.; Lin, Z.; Wu, G. Mode characteristics and reconstruction of flow field around two tandem circular cylinders. *J. Harbin Inst. Technol.* **2022**, *54*, 49–57.
9. Zhu, H.; Yao, Q.; Kanayama, H. Large-Scale Computations of Flow around Two Cylinders by a Domain Decomposition Method. *Math. Probl. Eng.* **2016**, *2016 Pt 3*, 4126123.1–4126123.8. [CrossRef]
10. Deng, Y.; Yin, G.; Zhou, L.; Xi, G. Effect of spacing ratio on flow passed two circular cylinders in tandem arrangements near wall via experiment. *Mach. Des. Manuf.* **2022**, *380*, 174–177, 181.
11. Zhao, K.; Wang, Z.; Cen, W.; Long, X. Application of lattice Boltzmann method in flow past two cylinders in tandem arrangement. *J. Ship Mech.* **2018**, *22*, 144–155.
12. Zou, L.; Guo, C.; Xiong, C. Flow characteristics of the two tandem wavy cylinders and drag reduction phenomenon. *J. Hydrodyn.* **2013**, *25*, 737–746. [CrossRef]
13. Zhang, Y.; Luo, L.; Chen, W. Numerical simulation of flow around two parallel cylinders with unequal diameters. *Ship Sci. Technol.* **2021**, *43*, 48–52.
14. Lin, L.; Chen, W.; Lin, Y.; Li, Y. Numerical simulation of the characteristics and interaction of flow around two side-by-side arranged circular cylinders. *Chin. J. Appl. Mech.* **2021**, *38*, 844–850.
15. Li, Y.; Su, Z.; Li, X. Three-dimensional numerical simulation of flow around two side-by-side cylinders at high Reynolds numbers using DES method. *Chin. J. Hydrodyn.* **2014**, *29*, 412–420. [CrossRef]
16. Du, X.; Lin, W.; Shi, C.; Sun, Y. Large eddy simulation of flow around two side-by-side circular cylinders at a high Reynolds number. *J. Harbin Inst. Technol.* **2019**, *51*, 193–200.
17. Chen, W.-L.; Xu, F. Investigation of a hybrid approach combining experimental tests and numerical simulations to study vortex-induced vibration in a circular cylinder. *J. Sound Vib.* **2012**, *331*, 1164–1182. [CrossRef]
18. Ma, W.; Jiang, Y.; Yu, Y. The numerical simulation of flow around two circular cylinders. *J. Fudan Univ. Nat. Sci.* **2013**, *52*, 592–600.
19. Harichandan, A.B.; Roy, A. Numerical investigation of low Reynolds number flow past two and three circular cylinders using unstructured grid CFR scheme. *Int. J. Heat Fluid Flow* **2010**, *31*, 154–171. [CrossRef]
20. Tan, Z.; Xiong, M.; Wang, Y. LES on flow past three tandem cylinders at high Reynolds number. *Port Waterw. Eng.* **2022**, *603*, 25–33.
21. Tu, J.; Wang, C.; Liang, J.; Deng, X.; Guo, X.; Zhang, P. Study on flow characteristics of three tandem cylinders at subcritical Reynolds number. *J. Ship Mech.* **2021**, *25*, 1159–1171.
22. Yang, Q.; Liu, Q.; Liu, X. Time averaged pressure distribution and aerodynamic force of flow around three circular cylinders. *J. Vib. Meas. Diagn.* **2019**, *39*, 1011–1015, 1133.
23. Zhang, Z.; Ji, C.; Xu, D.; Chen, W.; Yang, X. Response and wake characteristics of vortex-induced vibrations of three tandem circular cylinders with the upstream cylinder fixed. *Chin. J. Hydrodyn.* **2019**, *34*, 174–183.
24. *JTG D60-2015*; General Specifications for Design of Highway Bridges and Culverts. People's Communications Press: Beijing, China, 2015.
25. American Petroleum Institute. *Recommended Practice for Planning, Designing and Constructing Fixed Offshore Platforms-Working Stress Design*, 22nd ed.; American Petroleum Institute: Washington, DC, USA, 2014.
26. De Vanna, F.; Baldan, G.; Picano, F.; Benini, E. Effect of convective schemes in wall-resolved and wall-modeled LES of compressible wall turbulence. *Comput. Fluids* **2023**, *250*, 105710. [CrossRef]

27. De Vanna, F.; Bernardini, M.; Picano, F.; Benini, E. Wall-modeled LES of shock-wave/boundary layer interaction. *Int. J. Heat Fluid Flow* **2022**, *98*, 109071. [CrossRef]
28. Yang, Z. Large-eddy simulation: Past, present and the future. *Chin. J. Aeronaut.* **2015**, *28*, 11–24.
29. Chipongo, K.; Khiadani, M.; Sookhak Lari, K. Comparison and verification of turbulence Reynolds-averaged Navier–Stokes closures to model spatially varied flows. *Sci. Rep.* **2020**, *10*, 19059. [CrossRef]
30. Hanjalic, K. Will RANS survive LES? A view of perspectives. *J. Fluids Eng.* **2005**, *127*, 831. [CrossRef]
31. Lamberti, L. Data Driven Modelling of Turbulent Flows Using Artificial Neural Networks. Master's Thesis, University of Illinois, Chicago, IL, USA, 2020.
32. Nguyen, T.H.T.; Ahn, J.; Park, S.W. Numerical and Physical Investigation of the Performance of Turbulence Modeling Schemes around a Scour Hole Downstream of a Fixed Bed Protection. *Water* **2018**, *10*, 103. [CrossRef]
33. Wornom, S.; Ouvrard, H.; Salvetti, M.V.; Koobus, B.; Dervieux, A. Classical and variational multiscale Large-Eddy simulations of the flow around a circular cylinder on unstructured grids. *Comput. Fluids* **2010**, *39*, 1083–1094.
34. Meyer, M.; Hickel, S.; Adams, N.A. Assessment of implicit Large-Eddy simulation with a conservative immersed interface method for turbulent cylinder flow. *Int. J. Heat Fluid Flow* **2010**, *31*, 368–377. [CrossRef]
35. Hu, Z.; Liu, H.; Chen, N.; Hu, J.; Tong, F. Vortex shedding noise and flow mode analysis of cylinder with full/partial porous coating. *Aerosp. Sci. Technol.* **2020**, *106*, 106154. [CrossRef]
36. Norberg, C. Fluctuating lift on a circular cylinder: Review and new measurements. *J. Fluids Struct.* **2003**, *17*, 57–96. [CrossRef]
37. Khalak, A.; Williamson, C.H.K. Dynamics of a Hydroelastic Cylinder with Very Low Mass and Damping. *J. Fluids Struct.* **1996**, *10*, 455–472. [CrossRef]
38. *JTS 144-1-2010*; Load Code for Harbour Engineering. People's Communications Press: Beijing, China, 2010.
39. *JTGT3650-2020*; Technical Specifications for Construction of Highway Bridges and Culverts. People's Communications Press: Beijing, China, 2020.
40. Luo, C.; Ding, B.; Tian, Z.; Cong, P.; Cao, H.; Dai, Y. Study on the Influence of Sheet Pile Cofferdam Based on Different Flow Pressure Theories. *Eng. Technol. Ningxia* **2021**, *20*, 162–166.

Disclaimer/Publisher's Note: The statements, opinions and data contained in all publications are solely those of the individual author(s) and contributor(s) and not of MDPI and/or the editor(s). MDPI and/or the editor(s) disclaim responsibility for any injury to people or property resulting from any ideas, methods, instructions or products referred to in the content.